

Observational Constraint on Heavy Element Production in Inhomogeneous Big Bang Nucleosynthesis

Riou Nakamura ^{*,1} Masa-aki Hashimoto,¹ Shin-ichiro
Fujimoto,² Nobuya Nishimura,³ and Katsuhiko Sato^{4,5}

¹*Department of Physics, Faculty of Sciences,
Kyushu University, Fukuoka 812-8581, Japan*

²*Department of Control and Information Systems Engineering,
Kumamoto National College of Technology, Kumamoto 861-1102, Japan*

³*National Astronomical Observatory, 2-21-1,
Osawa, Mitaka, Tokyo 181-8588, Japan*

⁴*Institute for the Physics and Mathematics of the Universe,
The University of Tokyo, Chiba, 277-8568, Japan*

⁵*School of Science and Engineering,
Meisei University, Tokyo 191-8506, Japan*

(Dated: July 6, 2010)

Abstract

Based on a scenario of the inhomogeneous big-bang nucleosynthesis (IBBN), we investigate the detailed nucleosynthesis that includes the production of heavy elements beyond ${}^7\text{Li}$. From the observational constraints on light elements of ${}^4\text{He}$ and D for the baryon-to-photon ratio given by WMAP, possible regions found on the plane of the volume fraction of the high density region against the ratio between high- and low-density regions.

In these allowed regions, we have confirmed that the heavy elements beyond Fe can be produced appreciably, where p - and/or r -process elements are produced well simultaneously compared to the solar system abundances. We suggest that recent observational signals such as ${}^4\text{He}$ overabundance in globular clusters and high metallicity abundances in quasars could be partly due to the results of IBBN. Possible implications are given for the formation of the first generation stars.

PACS numbers: 26.35.+c, 98.80.Ft, 13.60.Rj

* E-mail: riou@phys.kyush-u.ac.jp

I. INTRODUCTION

Big bang nucleosynthesis has been investigated mainly on the context of the standard cosmological model (SBBN), where origin of light elements of ^4He , D, and ^7Li have been discussed in detail [1]. While observations of ^4He are still in debate with the uncertainty of 20-30 % in the abundance [2–4], those of D constrain severely the possible range of the abundance production in the early universe [5–7]. Contrary to the above standard BBN, the heavy element nucleosynthesis beyond the mass number $A = 8$ has been proposed from twenty years ago [8–14], where the model is called the inhomogeneous BBN (IBBN). This model relays on the inhomogeneity of baryon concentrations that could be induced by baryogenesis (e.g. Ref. [14]) or some phase transitions such as QCD or electro-weak phase transition [8, 15, 16] during the expansion of the universe. Although a large scale inhomogeneity is inhibited by many observations [17, 18], small scale one has been advocated within the present accuracy of the observations. Therefore, it remains a possibility for IBBN to occur in some degree during the early era.

On the other hand, Wilkinson Microwave Anisotropy Probe (WMAP) has derived critical parameters concerning the cosmology of which the present baryon-to-photon ratio η is determined to be $\eta = (6.19 \pm 0.15) \times 10^{-10}$ [18]. This value is almost consistent with that obtained from the observation of D. Therefore, considering the uncertainty of the ^4He abundance, we can fix the ratio η in the discussion of the nucleosynthesis in the early universe. If the present ratio of η is determined, BBN can be performed along that line in the thermodynamical history with use of the nuclear reaction network. On the other hand, peculiar observations of abundances for heavy elements and/or ^4He could be understood in the way of IBBN. For example, the quasar metallicity of C, N, and Si could have been explained from IBBN [19]. Furthermore, from recent observations of globular clusters, possibility of inhomogeneous helium distribution is pointed out [36], where some separate groups of different main sequences in blue band of low mass stars are assumed due to high primordial helium abundances compared to the standard value [20, 21].

Despite a negative opinion against IBBN due to insufficient consideration of the scale of the inhomogeneity [22], Matsuura et al. have found that the heavy element synthesis for both p - and r -processes is possible if $\eta > 10^{-4}$ [23], where they have also shown that the high η regions are compatible with the observations of the light elements, ^4He and

D [24]. However, their analysis is only limited to a parameter of a specific baryon number concentration. Therefore, it should be needed to constrain the possible regions from available observations in the wide parameter space that describes the IBBN.

In §II, we review and give the adopted model of IBBN [24]. Constraints on the critical parameters of IBBN due to light element observations are shown in §III, and the productions of possible heavy element nucleosynthesis is presented in §IV. Finally, §V is devoted to the summary and discussion.

II. COSMOLOGICAL MODEL

We adopt the two-zone model for the inhomogeneous BBN, where the early universe is assumed to have the high- and low- baryon density regions [12] under the background temperature T . For simplicity we ignore the diffusion effects before ($10^{10}\text{K} < T < 10^{11}\text{K}$) and during the primordial nucleosynthesis ($10^7\text{K} < T < 10^{10}\text{K}$), where the plausibility will be discussed in §V. After the epoch of BBN, all the elements are assumed to be mixed homogeneously.

Let us define the notations, n_{ave} , n_{high} , and n_{low} as averaged-, high-, and low- baryon number densities. f_v is the volume fraction of the high baryon density region. X_i^{ave} , X_i^{high} and X_i^{low} are mass fractions of each element i in averaged-, high- and low-density regions, respectively. Then, basic relations are written as follows:

$$n_{ave} = f_v n_{high} + (1 - f_v) n_{low}, \quad (1)$$

$$n_{ave} X_i^{ave} = f_v n_{high} X_i^{high} + (1 - f_v) n_{low} X_i^{low}. \quad (2)$$

Here we assume the baryon fluctuation to be isothermal as was done in previous studies (e.g., Refs. [8, 9, 15]). Under that assumption, since the baryon-to-photon ratio is defined by the number density of photon in standard BBN, $n_\gamma = 2\zeta(3)/\pi^2 (k_B T/\hbar c)^3$, Eqs.(1) and (2) are rewritten as follows:

$$\eta_{ave} = f_v \eta_{high} + (1 - f_v) \eta_{low}, \quad (3)$$

$$\eta_{ave} X_i^{ave} = f_v X_i^{high} \eta_{high} + (1 - f_v) X_i^{low} \eta_{low}, \quad (4)$$

where η s with subscripts are the baryon-to-photon ratios in each region. In the present paper, we fix $\eta_{ave} = 6.1 \times 10^{-10}$ from the cosmic microwave background observation [17, 18].

η_{high} and η_{low} are obtained from both f_v and the density ratio between high- and low-density region: $R \equiv n_{high}/n_{low} = \eta_{high}/\eta_{low}$.

To calculate the evolution of the universe, we solve the following Friedmann equation,

$$\left(\frac{\dot{x}}{x}\right)^2 = \frac{8\pi G}{3}\rho, \quad (5)$$

where x is the cosmic scale factor and G is the gravitational constant. The total energy density ρ is the sum of decomposed parts:

$$\rho = \rho_\gamma + \rho_{e^\pm} + \rho_\nu + \rho_b.$$

Here the subscripts γ, e^\pm, ν , and b indicate photons, electrons/positrons, neutrinos, and baryons, respectively. We note that ρ_b is the average value of baryon density obtained from Eq. (1).

The energy conservation law is used to get the time evolution of the temperature and the baryon density,

$$\frac{d}{dt}(\rho x^3) + p \frac{d}{dt}(x^3) = 0, \quad (6)$$

where p is the pressure of the fluid.

III. CONSTRAINTS FROM LIGHT-ELEMENT OBSERVATIONS

In this section, we calculate the nucleosynthesis in high- and low-density regions with use of the BBN code [27] which includes 24 nuclei from neutron to ^{16}O . We adopt the reaction rates of NACRE [31], the neutron life time $\tau_N = 885.7$ sec [33], and take account of the number of species of the massless neutrinos $N_\nu = 3$.

Figure 1 illustrates the light element synthesis in the high- and low-density regions with $f_v = 10^{-6}$ and $R = 10^6$ that correspond to $\eta_{high} = 3.05 \times 10^{-4}$ and $\eta_{low} = 3.05 \times 10^{-10}$. In the low-density region the evolution of the elements is almost the same as that of standard BBN. In the high-density region, while ^4He is more abundant than that in the low-density region, ^7Li (or ^7Be) is much less produced. It implies that heavier nuclei such as ^{16}O , hardly synthesized in SBBN, are synthesized at high-density region.

For $f_v \ll 0.1$, the heavier elements can be synthesized in the high-density regions as discussed in Ref. [13]. For $f_v > 0.1$, contribution of the low-density region to η_{ave} can be neglected and therefore to be consistent with observations of light elements, we need to

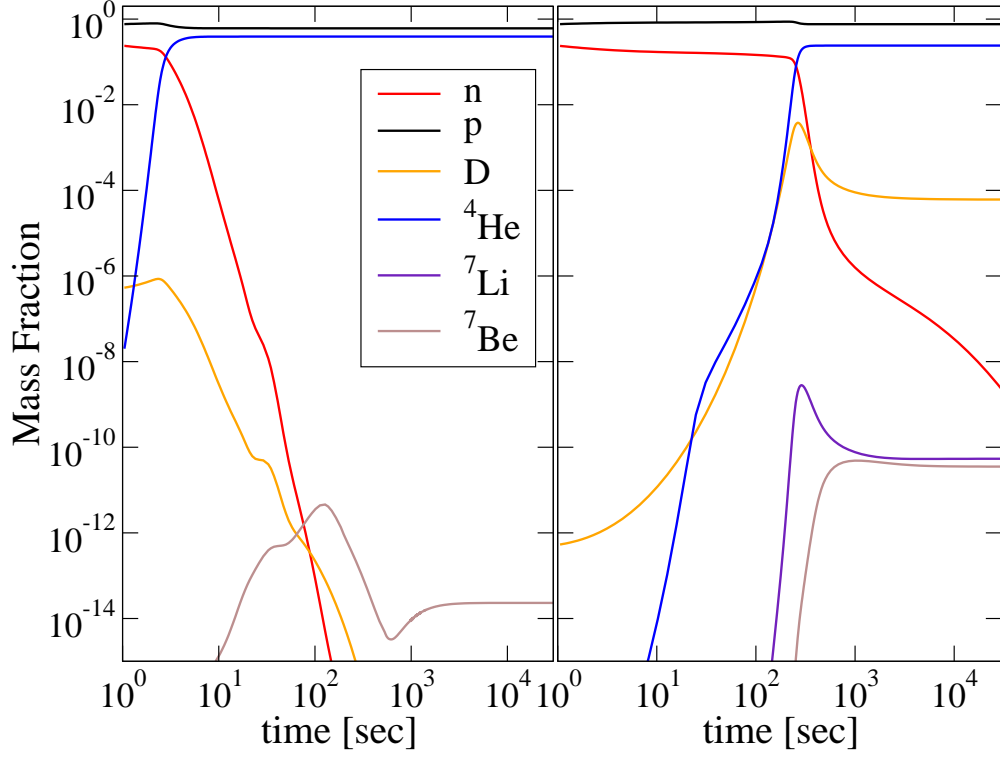


Fig. 1: Illustration of the nucleosynthesis in the two-zone IBBN model with $f_v = 10^{-6}$ and $R = 10^6$. The baryon-to-photon ratios in the high- (left panel) and low- (right panel) density regions are $\eta_{high} = 3.05 \times 10^{-4}$ and $\eta_{low} = 3.05 \times 10^{-10}$, respectively.

impose the condition of $f_v < 0.1$. Now, we put constraints on f_v and R by comparing the average values of ${}^4\text{He}$ and D obtained from Eq. (4) with the following observational values. First we adopt the primordial ${}^4\text{He}$ abundance reported in Ref. [4]:

$$0.232 < Y_p < 0.258. \quad (7)$$

Next, we take the primordial abundance from the D/H observation reported in Ref. [28]

$$\text{D}/\text{H} = (2.84 \pm 0.26) \times 10^{-5}, \quad (8)$$

where the systematic error given in Ref. [7] is adopted.

Figure 2 illustrates the constraints on the $f_v - R$ plane from the above light-element observations with contours of constant η_{high} . The solid and dashed lines indicate the upper limits from Eqs. (7) and (8), respectively. As the results, we can obtain approximately the

following relations between f_v and R :

$$R \leq \begin{cases} 0.26 \times f_v^{-0.96} & \text{for } f_v > 3.2 \times 10^{-6}, \\ 1.20 \times f_v^{-0.83} & \text{for } f_v \leq 3.2 \times 10^{-6}. \end{cases} \quad (9)$$

As shown in Figure 2, we can find the allowed regions which include the very high-density region such as $\eta_{high} = 10^{-3}$.

Matsuura et al. [24] defined a parameter of the baryon number concentration a in the high density region instead of two parameters of f_v and R that are needed to solve Eqs.(3) and (4):

$$f_v \eta_{high} : (1 - f_v) \eta_{low} = a : (1 - a).$$

However, they have only examined the case of $\eta_{high} = 10^{-3}$ and $\eta_{low} = 3.162 \times 10^{-10}$, where $a = 0.48$ for $\eta_{ave} = 6.1 \times 10^{-10}$. Our constraints in Eq. (9) correspond to $a = 0.02 - 0.5$. Since we have fixed the value of η_{ave} , we can obtain physically more reasonable regions on the plane of (f_v, R) .

Naturally, as η_{high} takes larger value, nuclei which are heavier than ${}^7\text{Li}$ are synthesized more and more. Then we can estimate the amount of total CNO elements in the allowed region. Figure 3 illustrates the contours of the summation of the average values of the heavier nuclei ($A > 7$), which correspond to Fig. 2 and are drawn using the constraint from ${}^4\text{He}$ and D/H observations. As a consequence, we get the upper limit of total mass fractions for heavier nuclei as follows: $X(A > 7) \leq 10^{-7}$.

We should note that abundance flows proceed beyond the CNO elements thanks to the larger network for high η -values as shown in Table II of the following section.

IV. HEAVY ELEMENT PRODUCTION

In the previous section, we have obtained the amount of CNO elements produced in the two-zone IBBN model. However, it is not enough to examine the nuclear production beyond $A > 8$ because the baryon density in the high-density region becomes so high that elements beyond CNO isotopes can be produced [10, 14, 23, 34].

In this section, we investigate the heavy element nucleosynthesis in the high-density region considering the constraints shown in Fig. 2. The temperature and density evolutions are the same as used in the previous section. Abundance change is calculated with a large nuclear

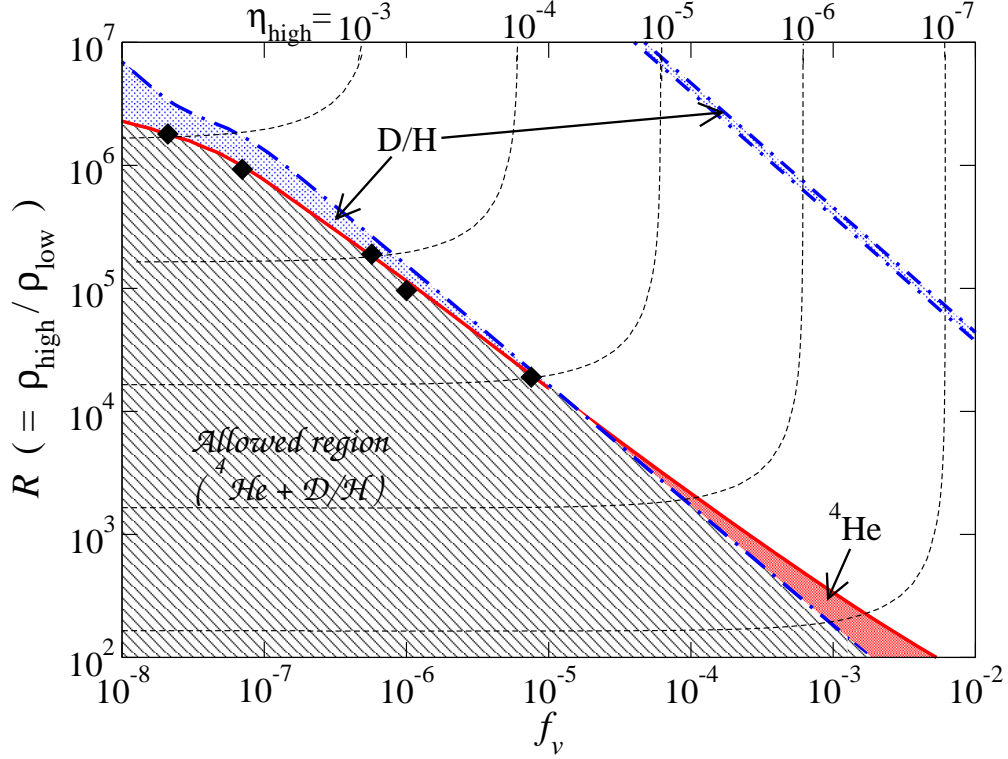


Fig. 2: Constraints on the $f_v - R$ plane from the observations of light element abundances. The region below the solid line is allowed one obtained from ${}^4\text{He}$ observation [4]. Constraints from the D/H observation [28] are shown by the region below the dot-dashed line. The shaded region is the allowed parameters determined from the two observations of ${}^4\text{He}$ and D/H. The dotted lines show the contours of the baryon-to-photon ratio in the high-density region. Filled squares indicate the parameters for heavy element nucleosynthesis adopted in §IV.

reaction network, which includes 4463 nuclei from neutron (n), proton (p) to Americium ($Z = 95$ and $A = 292$). Nuclear data, such as reaction rates, nuclear masses, and partition functions, are the same as used in [26] except for the neutron-proton interaction; We take the weak interaction rates between n and p from Kawano code [29], which is adequate for the high temperature epoch of $T > 10^{10}$ K. We note that mass fraction of ${}^4\text{He}$ and D obtained with the large network are consistent with those in §III within the accuracy of few percents.

As seen in Fig. 3, heavy elements of $X(A > 7) > 10^{-9}$ are produced nearly along the upper limit of R . Therefore, to examine the efficiency of the heavy element production, we select five models with the following parameters: $\eta_{\text{high}} = 10^{-3}, 5.3 \times 10^{-4}, 10^{-4}, 5.5 \times 10^{-5}$

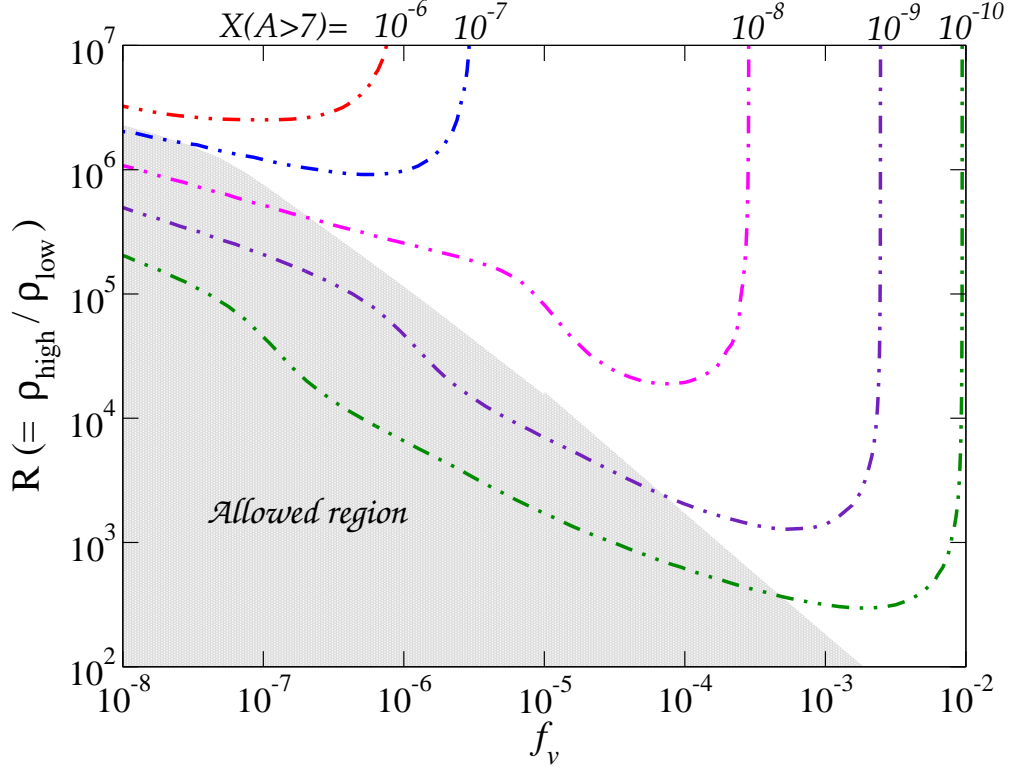


Fig. 3: Contours of the averaged total mass fractions which are the sum of nuclei heavier than ${}^7\text{Li}$, where we find consistent regions with ${}^4\text{He}$ and D observations.

, and 10^{-5} corresponded to $(f_v, R) = (2.1 \times 10^{-8}, 1.8 \times 10^6)$, $(7.0 \times 10^{-8}, 9.3 \times 10^5)$, $(5.7 \times 10^{-7}, 1.9 \times 10^5)$, $(1.0 \times 10^{-6}, 9.6 \times 10^4)$, and $(7.5 \times 10^{-6}, 1.9 \times 10^4)$. Adopted parameters are indicated by filled squares in Fig. 2.

Figure 4 shows the results of nucleosynthesis in the high-density regions with $\eta_{\text{high}} \simeq 10^{-4}$ and 10^{-3} . For $\eta_{\text{high}} \simeq 10^{-4}$, the nucleosynthesis paths are classified with the mass number [23]. For nuclei of mass number $A \leq 100$, proton captures are very active compared to the neutron capture of $T > 2 \times 10^9$ K and the path moves to the proton rich side, which began by breaking out of the hot CNO cycle. For nuclei of $100 < A < 120$, the path goes across the stable nuclei from proton to neutron rich side, since the temperature decreases and the number of seed nuclei of the neutron capture process increase significantly. Concerning heavier nuclei of $A \geq 120$, neutron captures become much more efficient. In Figure 4(a), we see the time evolution of the abundances of Gd and Eu for the mass number 159. First ${}^{159}\text{Tb}$ (stable r -element) is synthesized and later ${}^{159}\text{Gd}$ and ${}^{159}\text{Eu}$ are synthesized through the neutron captures. After $t = 10^3$ sec, ${}^{159}\text{Eu}$ decays to nuclei by way of ${}^{159}\text{Eu} \rightarrow {}^{159}\text{Gd}$

$\rightarrow {}^{159}\text{Tb}$, where the lifetimes of ${}^{159}\text{Eu}$ and ${}^{159}\text{Gd}$ are 10.1 min and 18.479 h, respectively. These neutron capture process is not similar to the canonical r -process, since the nuclear processes proceed under the condition of the high-abundance of protons.

For $\eta_{\text{high}} \simeq 10^{-3}$, the reactions first proceed along the stable line, because triple- α reactions and other particle induced reactions are very effective. Subsequently, the reactions directly proceeds to the proton rich region, through rapid proton captures. As shown in Fig. 4(b), ${}^{108}\text{Sn}$ which is proton-rich nuclei is synthesized. After that, stable nuclei ${}^{108}\text{Cd}$ is synthesized by way of ${}^{108}\text{Sn} \rightarrow {}^{108}\text{In} \rightarrow {}^{108}\text{Cd}$, where the lifetimes of ${}^{108}\text{Sn}$ and ${}^{108}\text{In}$ are 10.3 min and 58.0 min, respectively. In addition, we notice the production of radioactive nuclei of ${}^{56}\text{Ni}$ and ${}^{57}\text{Co}$, where ${}^{56}\text{Ni}$ is produced at early times, just after the formation of ${}^4\text{He}$. Usually, nuclei such as ${}^{56}\text{Ni}$ and ${}^{57}\text{Co}$ are produced in supernova explosions, which are assumed to be the events after the first star formation (e.g. Ref. [32]). In IBBN model, however, this production can be found to occur at extremely high density region of $\eta_{\text{high}} \geq 10^{-3}$ as the primary elements without supernova events in the early universe.

To explain differences of the nuclear reactions which depend on the baryon density, we focus on the neutron abundances. Figure 5 shows the evolutions of the neutron abundances in the SBBN and IBBN models. For $\eta_{\text{high}} = 10^{-3}$, neutron abundance decreases rapidly at ~ 10 sec to the formation of ${}^4\text{He}$ and ${}^{56}\text{Ni}$. Thus, neutron abundance is not enough to induce the neutron capture producing heavy nuclei of $A > 90$. On the other hand, neutron abundance tends to remain even at the high temperature for the lower value of η_{high} . We can see the case of $\eta_{\text{high}} = 10^{-4}$, where there remain much neutrons to occur the neutron capture reaction. Thus the neutron capture process to produce heavy elements of $A > 90$ can become active.

Time scales in the decrease for the neutron abundances change drastically the flow of the abundance production. Figures 6 and 7 show the flows for $\eta_{\text{high}} = 5.3 \times 10^{-4}$. Before the significant decrease in the neutron abundances before 10 sec, the nucleosynthesis proceeds already along the stable line by way of the neutron included reactions (Fig. 6). At that time, the nuclear reactions are stuck around $Z = 60$ with $N = 82$, since it takes time to synthesize heavier nuclei because Nd ($Z = 60$) and Sm ($Z = 62$) have some stable isotopes. As time goes, neutron captures of these nuclei start, where the neutron captures proceed significantly and r -elements can be synthesized. After the depletion of neutrons ($t > 40$ sec), nuclei around the neutron numbers $N = 82$ are produced through proton induced reactions

such as ^{144}Sm (Fig. 7).

Final results ($T = 4 \times 10^7$ K) of nucleosynthesis calculations are shown in Tables I and II. Table I shows the abundances of light elements, ^4He , D, and ^7Li , in high- and low-density regions with their average values. Abundances of the low-density side (the third and sixth columns) are obtained from the calculation by BBN code used in §III, because abundance flows beyond $A = 7$ are negligible. We should note that the average abundances of ^4He and D are consistent with their observational values of (7) and (8). Table II shows the amounts of heavy elements. When we have calculate the average values, we set the abundances of $A > 16$ as zero for low-density side. For $\eta_{\text{high}} \simeq 10^{-4}$, a lot of nuclei of $A > 7$ are synthesized whose amounts are comparable to that of ^7Li . Produced elements in this case include both s -element (i.e. ^{138}Ba) and r -elements (for instance, ^{142}Ce and ^{148}Nd), since moderate amounts of neutrons remain as shown in Fig. 5

For $\eta_{\text{high}} \simeq 10^{-3}$, there are few r -elements while both s -elements (i.e. ^{82}Kr and ^{89}Y) and p -elements (i.e. ^{74}Se and ^{78}Kr) are synthesized such as the case of supernova explosions. Although heavy nuclei of $A \geq 100$ are not synthesized appreciably, those of $A \leq 90$ are produced well owing to the explosive nucleosynthesis under the high density circumstances ($\rho \sim 10^6$ g cm $^{-3}$). The most abundant element is found to be ^{56}Ni whose production value is much larger than the estimated upper limit of the total mass fraction (shown in Fig.3) derived from the BBN code calculations. This is because our BBN code used in §III includes the elements up to $A = 16$ and the actual abundance flow proceeds to much heavier elements.

Figure 8 shows the abundances averaged between high- and low-density region using Eq. (4) compared with the solar system abundances [30]. For $\eta_{\text{high}} \simeq 10^{-4}$, abundance productions of $120 < A < 180$ are comparable to the solar values. For $\eta_{\text{high}} \simeq 10^{-3}$, those of $50 < A < 100$ have been synthesized well. In the case of $\eta_{\text{high}} = 5.3 \times 10^{-4}$, there are outstanding two peaks; one is around $A = 56$ ($N = 28$) and the other can be found around $A = 140$. Abundance patterns are very different from that of the solar system, because IBBN occurs under the condition of significant abundances of both neutrons and protons.

V. SUMMARY AND DISCUSSION

We have investigated the consistency between inhomogeneous BBN and the observation of ^4He and D/H abundances under the standard cosmological model having η determined

Table. I: Mass fractions of light elements for follow cases : $\eta_{high} \simeq 10^{-3}$, $\eta_{high} = 5 \times 10^{-4}$, $\eta_{high} \simeq 10^{-4}$, and $\eta_{high} = 10^{-5}$. t_{fin} and T_{fin} is the time and temperature at the final stage of the calculations.

f_v, R	$2.1 \times 10^{-8}, 1.8 \times 10^6$			$7.0 \times 10^{-8}, 9.3 \times 10^5$		
$(\eta_{high}, \eta_{low})$	$(1.06 \times 10^{-3}, 5.88 \times 10^{-10})$			$(5.33 \times 10^{-4}, 5.73 \times 10^{-10})$		
(t_{fin}, T_{fin})	$1.0 \times 10^5 \text{sec}, 4.2 \times 10^7 \text{ K}$			$1.1 \times 10^5 \text{sec}, 4.9 \times 10^7 \text{ K}$		
elements	high	low	average	high	low	average
p	0.586	0.753	0.746	0.598	0.753	0.743
D	1.76×10^{-21}	4.48×10^{-5}	4.32×10^{-5}	4.14×10^{-21}	4.67×10^{-5}	4.38×10^{-5}
^4He	0.413	0.247	0.253	0.402	0.247	0.257
^7Li	1.63×10^{-13}	1.79×10^{-9}	1.72×10^{-9}	3.43×10^{-13}	1.70×10^{-9}	1.59×10^{-9}
(a) For cases of $\eta_{high} = 10^{-3}$ and $\eta_{high} = 5 \times 10^{-4}$.						
f_v, R	$1.0 \times 10^{-7}, 1.7 \times 10^5$			$7.5 \times 10^{-6}, 1.9 \times 10^4$		
$(\eta_{high}, \eta_{low})$	$(1.02 \times 10^{-4}, 6.00 \times 10^{-10})$			$(1.02 \times 10^{-5}, 5.34 \times 10^{-10})$		
(t_{fin}, T_{fin})	$1.2 \times 10^5 \text{sec}, 4.3 \times 10^7 \text{ K}$			$1.2 \times 10^5 \text{sec}, 4.5 \times 10^7 \text{ K}$		
elements	high	low	average	high	low	average
p	0.638	0.752	0.750	0.670	0.753	0.743
D	6.84×10^{-22}	4.34×10^{-5}	4.27×10^{-5}	1.12×10^{-22}	5.19×10^{-5}	4.55×10^{-5}
^4He	0.362	0.248	0.249	0.330	0.246	0.257
^7Li	7.42×10^{-13}	1.87×10^{-9}	1.70×10^{-9}	6.73×10^{-8}	1.47×10^{-9}	9.63×10^{-9}
(b) For cases of $\eta_{high} = 10^{-4}$ and $\eta_{high} = 10^{-5}$.						

by WMAP. We have adopted the two-zone model, where the universe has the high- and low-baryon density regions at the BBN epoch.

First, we have calculated the light element nucleosynthesis using the BBN code having 24 nuclei for the high- and low-density regions. We have assumed that the diffusion effect is negligible. There are significant differences for the time evolution of the light element between the high- and low-density regions; In the high-density region, the nucleosynthesis begins faster and ^4He is more abundant than that in the low density region as shown in Figure 4. From ^4He and D/H observations, we can put severe constraint on two parameters of the two-zone model: the volume fraction f_v of the high-density region and the density

ratio R between the two regions, where we have assumed that abundances in the two regions are mixed homogeneously.

Second, using the allowed parameters constrained from the light element observations, we calculate the nucleosynthesis that includes 4463 nuclei in the high-density regions. Qualitatively, results of nucleosynthesis are the same as those in Ref. [23]. In the present results, we showed that p - and r -elements are synthesized simultaneously at high-density region with $\eta_{high} \simeq 10^{-4}$. Such a curious site of the nucleosynthesis have never been known in previous studies of nucleosynthesis.

As the results, we have obtained the average values of mass fractions from the nucleosynthesis in high-density and that in low density regions. The total averaged mass fractions beyond the light elements $X(A > 7)$ are constrained to be 10^{-5} (for $\eta_{high} = 10^{-3}$) and 10^{-7} (for $\eta_{high} = 10^{-4}$). We find that the average mass fractions in IBBN amount to as much as the solar system abundances. As seen from Fig. 8, there are over-produced elements around $A = 150$ (for $\eta_{high} = 10^{-4}$) and $A = 80$ (for $\eta_{high} = 10^{-3}$). It seems to be conflict with the chemical evolution of the universe. However, we show only the results of the upper-bounds on $f_v - R$ diagram. Since f_v and R are free-parameters, over-production can be avoided by the adjustment of f_v and/or R . Figure 9 illustrates the mass fraction in $\eta_{high} = 1.0 \times 10^{-4}$ with various $f_v - R$ sets. It is shown that the abundance pattern can be lower than the solar system abundance. Although we showed here only the result of $\eta_{high} = 10^{-4}$ case, it is possible to avoid producing over-abundance in other parameters, $\eta_{high} = 10^{-3}$ and $\eta_{high} = 5 \times 10^{-4}$. If we put constraint on the $f_v - R$ plane from the heavy element observations, the limit of those parameters should be tightly.

In our calculation, the radioactive nuclei are produced much in the high-density region. Especially, we should note that ^{56}Ni decays into ^{56}Fe ($^{56}\text{Ni} \rightarrow ^{56}\text{Co} \rightarrow ^{56}\text{Fe}$), where the existence of ^{56}Fe surely affects the process of the formation of the first generation stars. Therefore, it may be also necessary for IBBN to be constrained from the star formation scenarios, because opacity change due to IBBN will affect them.

Recent observational signal of over-abundances of ^4He mass fractions in globular clusters could motivate the IBBN scenario toward the detailed modeling. The over-abundances of ^4He are suggested to be in the range of $0.3 - 0.4$ where estimated from the H-R diagram of the blue Main-Sequence of NGC2808 in Ref.[21]. If the origin of ^4He in globular clusters is due to IBBN, η must be greater than 10^{-4} in some regions during the epoch of BBN.

Then, the averaging procedure could be constrained from the more detailed observations of abundances. Since the history of changes in abundances has been investigated in detail through the chemical evolution of galaxies [35], further plausible constraints on the averaging process should be studied in the next step.

In our study, we ignore the diffusion effects. However, it is shown that the diffusion affects the primordial nucleosynthesis significantly [12]. Matsuura et al. [24] has estimated the size of the high-baryon density island to be $10^3 \text{ m} - 10^{15} \text{ m}$ at the BBN epoch. The upper bound is obtained from the maximum angular resolution of CMB and the lower is from the analysis of comoving diffusion length of neutron and proton given in Ref. [11]. In our case, we can estimate the scale of the high-density and the effects of the diffusion from f_v .

The neutron diffusion effects can be discussed with use of the results obtained in the previous section by comparing the scale of the high-density region with the diffusion length. The present value of the Hubble length is $H_0^{-1} = 1.28 \times 10^{26} \text{ m}$. We may estimate the scale of the high-density region from the Hubble length H^{-1} multiplied by $f_v^{1/3}$. From ranges of the volume fraction adopted in §IV, $10^{-8} < f_v < 10^{-5}$, we obtain the scale of the high-density regions at present epoch d_0 as $2.7 \times 10^{23} \text{ m} < d_0 < 2.7 \times 10^{24} \text{ m}$. We can estimate the scale at redshift z from the relation $d(z) = d_0(1+z)^{-1}$. As the result, we expect d at BBN era ($z \sim 10^9$) as $2.7 \times 10^{14} \text{ m} < d_{BBN} < 2.7 \times 10^{15} \text{ m}$. We can say that the nucleon diffusion effects would be neglected because the diffusion length is much smaller than d .

On the other hand, the high-density region is expected to be smaller than 10^{15} m . It seems to be very bad that the upper bound of d is larger than the value as far as our two zone model is concerned. However, the high-density island cannot be observed directly, since we assume that the high- and low-density regions become homogeneous after the nucleosynthesis.

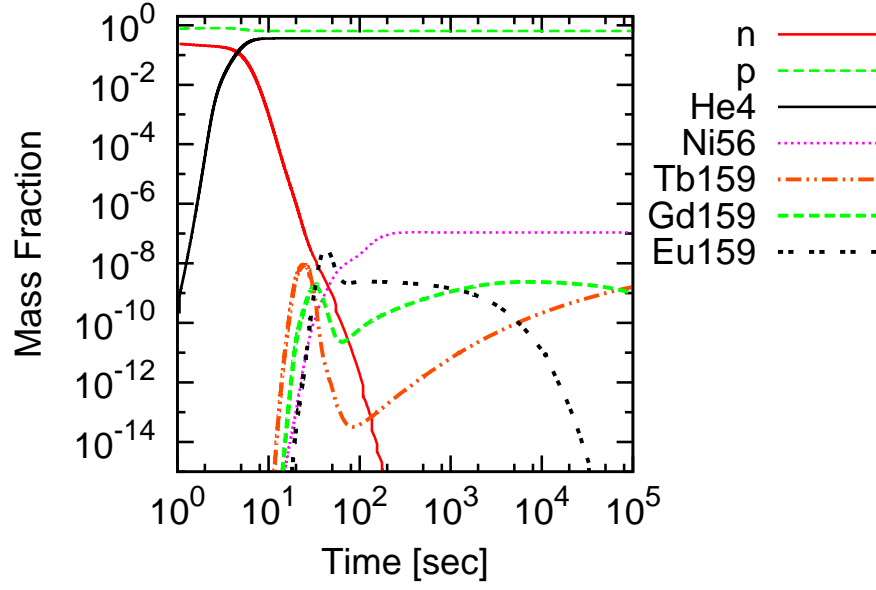
Finally, distances between high density regions are difficult to derive without specific models beyond the two-zone model. We will plan to calculate the nucleosynthesis with the diffusion of abundances and/or more plausible averaging process included.

Acknowledgments

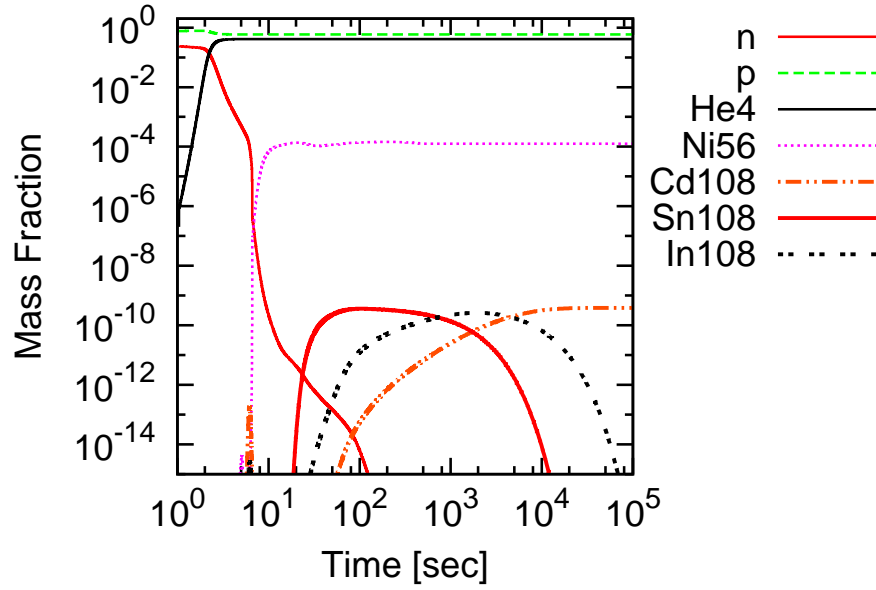
This work has been supported in part by a Grant-in-Aid for Scientific Research (18540279, 19104006, 21540272) of the Ministry of Education, Culture, Sports, Science and Technology of Japan, and in part by a grant for Basic Science Research Projects from the Sumitomo

- [1] G. Steigman, *Ann. Rev. Nucl. Part. Sci.* **57**, 463 (2007);
F. Iocco, G. Mangano, G. Miele, O. Pisanti and P. D. Serpico, *Phys. Rept.* **472**, 1 (2009)
- [2] V. Luridiana, A. Peimbert, M. Peimbert, & M. Cervino, *Astrophys. J.* **592**, 846 (2003)
- [3] Y. I. Izotov, T. X. Thuan and G. Stasinska, *Astrophys. J.* **662**, 15 (2007)
- [4] Olive & Skillman, *Astrophys. J.*, **617**, 29–40 (2004)
- [5] D. Kirkman, D. Tytler, N. Suzuki, J. M. O’Meara and D. Lubin, *Astrophys. J. Suppl.* **149**, 1 (2003) [arXiv:astro-ph/0302006].
- [6] M. Pettini, B. J. Zych, M. T. Murphy, A. Lewis, & C. C. Steidel, *Mon. Not. R. Astron. Soc.* **391**, 1499, (2008)
- [7] J. M. O’Meara, S. Burles, J. X. Prochaska, G. E. Prochter, R. A. Bernstein and K. M. Burgess, *Astrophys. J.* **649**, L61 (2006)
- [8] C. Alcock, G.M. Fuller, and G.J. Mathews, *Astrophys. J.* **320**, 439 (1987)
- [9] N. Terasawa and K. Sato, *Phys. Rev. D* **39**, 2893 (1989)
- [10] K. Jedamzik, and J.B. Rehm, *Phys. Rev.* **D64**, 023510 (2001)[astro-ph/0101292];
T. Rauscher, H. Applegate, J. Cowan, F. Thielmann, and M. Wiescher, *Astrophys. J.* **429**, 499 (1994).
- [11] J. H. Applegate, C. J. Hogan, and R. J. Scherrer, *Phys. Rev.* **D35**, 1151 (1987)
- [12] R. M. Malaney and W. A. Fowler, *Astrophys. J.* **333**, 14 (1988);
J. H. Applegate, C. J. Hogan, R. J. Scherrer, *Astrophys. J.* **329**, 572 (1988);
N. Terasawa and K. Sato, *Astrophys. J.* **362**, L47 (1990);
D. Thomas, D. N. Schramm, K.A. Olive, G. J. Mathews, B. S. Meyer, and B. D. Fields, *Astrophys. J.* **430**, 291 (1994);
- [13] K. Jedamzik, G. M. Fuller, G. J. Mathews, and T. Kajino, *Astrophys. J.* **422**, 423 (1994);
- [14] S. Matsuura, A. D. Dolgov, S. Nagataki and K. Sato, *Prog. Theor. Phys.* **112**, 971 (2004)
- [15] G. M. Fuller, G. J. Mathews and C. R. Alcock, *Phys. Rev. D* **37**, 1380 (1988);
- [16] H. Kurki-Suonio and R. A. Matzner, *Phys.Rev.* **D39**, 1046 (1989);
H. Kurki-Suonio and R. A. Matzner, *Phys.Rev.* **D42**, 1047 (1990);

- [17] C.L. Bennett, *et al.*, *Astrophys. J. Suppl.* **148**, 1 (2003)
D. N. Spergel *et al.*, *Astrophys. J. Suppl.* **170**, 377 (2007)
J. Dunkley *et al.* *Astrophys. J. Suppl.* **180**, 306 (2009)
- [18] E. Komatsu *et al.*, arXiv:1001.4538 [astro-ph.CO].
- [19] Y. Juarez, R. Maiolino, R. Mujica, M. Pedani, S. Marinoni, T. Nagao, A. Marconi, & E. Oliva, *Astron. & Astrophys.*, 494, L25, (2009)
- [20] L. R. Bedin *et al.*, *Astrophys. J.*, **605**, L125 (2004);
- [21] G. Piotto *et al.*, *Astrophys. J.*, **661** L53, (2007)
- [22] T. Rauscher, *Phys. Rev. D* **75**, 068301 (2007)
- [23] S. Matsuura, S. I. Fujimoto, S. Nishimura, M. A. Hashimoto and K. Sato, *Phys. Rev. D* **72**, 123505 (2005)
- [24] S. Matsuura, S. I. Fujimoto, M. A. Hashimoto and K. Sato, *Phys. Rev. D* **75**, 068302 (2007).
- [25] K. Jedamzik [astro-ph/9911242].
- [26] S. Fujimoto, M. Hashimoto, O. Koike, K. Arai, & R. Matsuba, *Astrophys. J.* **585**, 418 (2003),
O. Koike, M. Hashimoto, R. Kuromizu, & S. Fujimoto, *Astrophys. J.* **603**, 592 (2004),
S. Fujimoto, M. Hashimoto, K. Arai, & R. Matsuba, *Astrophys. J.* , **614**, 847 (2004),
S. Nishimura, K. Kotake, M. Hashimoto, S. Yamada, N. Nishimura, S. Fujimoto and K. Sato, *Astrophys. J.* **642**, 410 (2006).
- [27] M. Hashimoto & K. Arai, *Physics Reports of Kumamoto University*, **7**, 47, (1985).
- [28] B. Fields and S. Sarkar, arXiv:astro-ph/0601514.
- [29] L. Kawano, FERMILAB-Pub-92/04-A
- [30] E. Anders and N. Grevesse, *Geochim. Cosmochim. Acta* **53**, 197 (1989).
- [31] C. Angulo, M. Arnould, M. Rayet, P. Descouvemont, D. Baye, C. Leclercq-Willain, A. Coc, S. Barhoumi, P. Aguer, C. Rolfs, *et al.*, *Nuclear Physics A* 656, 3 (1999).
- [32] M. Hashimoto, *Progress of Theoretical Physics*, 94, 663, (1995).
- [33] K. Hagiwara *et al.* [Particle Data Group], *Phys. Rev. D* **66**, 010001 (2002).
- [34] R. V. Wagoner, W. A. Fowler, & F. Hoyle, *Astrophys. J.* , **148**, 3 (1967)
- [35] M. E. Anderson, J. N. Bregman, S. C. Butler and C. R. Mullis, *Astrophys. J.* **698**, 317 (2009)
- [36] T. Moriya and T. Shigeyama, *Phys. Rev. D* **81**, 043004 (2010)



(a) $\eta_{high} = 1.02 \times 10^{-4}$



(b) $\eta_{high} = 1.06 \times 10^{-3}$

Fig. 4: Time evolution of the mass fractions in high-density regions of (a) $\eta_{high} = 1.02 \times 10^{-4}$ and (b) $\eta_{high} = 1.06 \times 10^{-3}$.

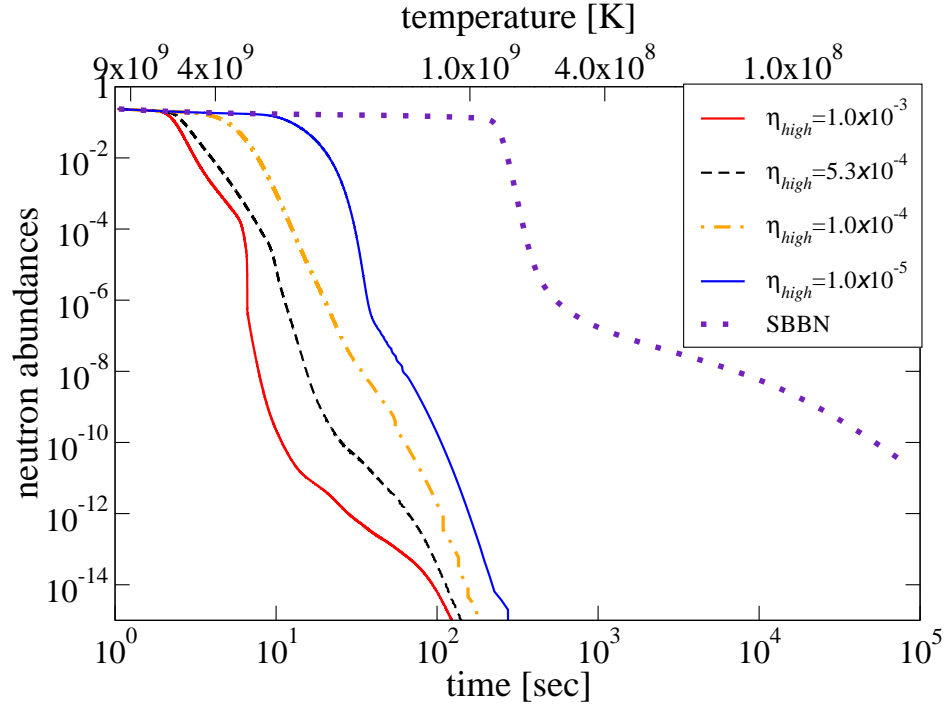


Fig. 5: Time evolution of the neutron abundance in SBBN ($\eta = 6.1 \times 10^{-10}$) and IBBN in the high-density region.

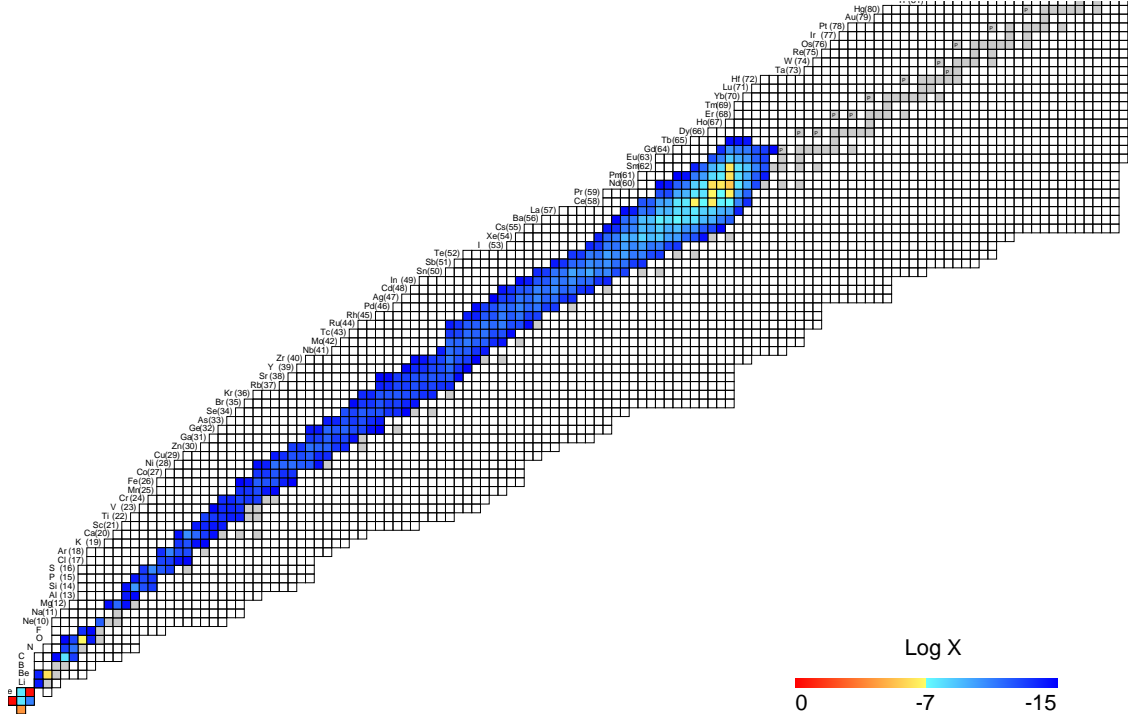


Fig. 6: Abundance distribution at $T = 3.5 \times 10^9$ K ($t \sim 9$ sec) in $\eta_{high} = 5.3 \times 10^{-4}$. The gray regions are those of stable nuclei.

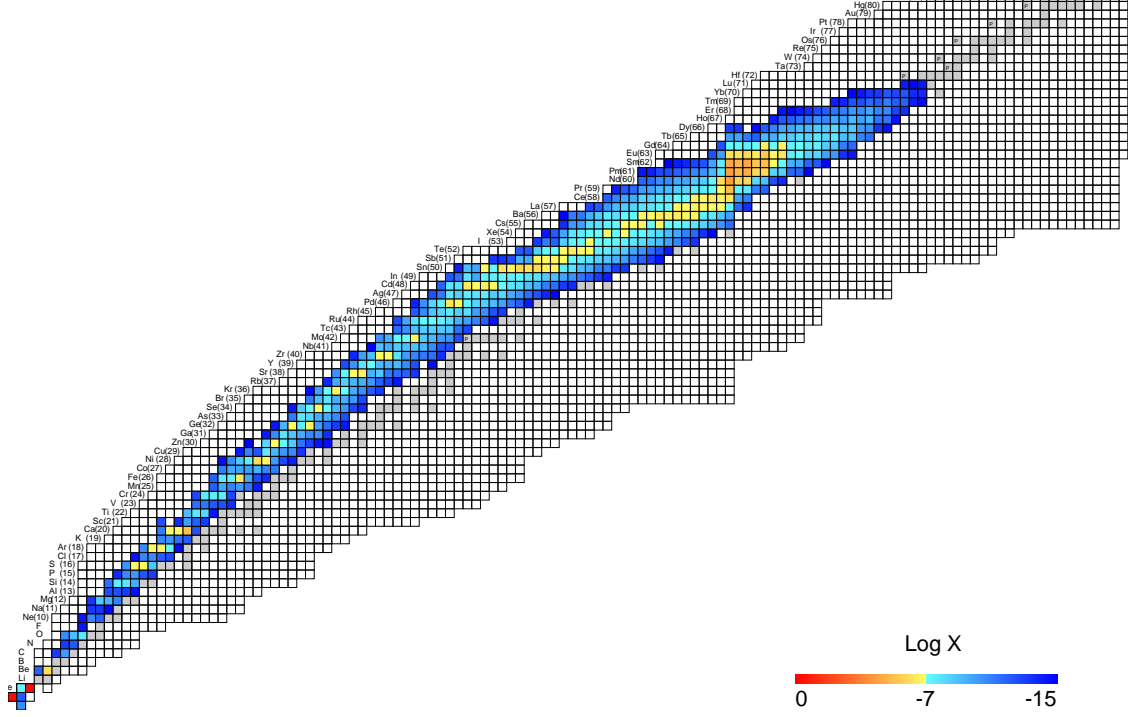


Fig. 7: . Abundances distribution at $T = 1.9 \times 10^9$ K ($t \sim 40$ sec) in $\eta_{high} = 5.3 \times 10^{-4}$.

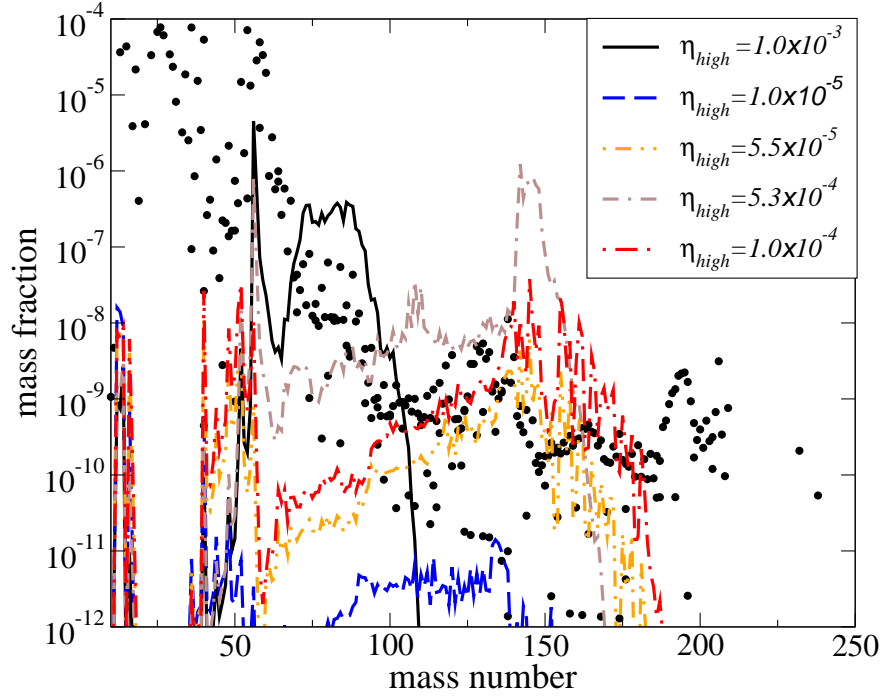


Fig. 8: Comparison of the averaged mass fractions in the two-zone model with the solar system abundances [30] (indicated by dots).

Table. II: Mass fractions of heavy elements ($A > 7$) for three cases of $\eta_{high} \simeq 10^{-3}$, $\eta_{high} = 5.33 \times 10^{-4}$, and $\eta_{high} \simeq 10^{-4}$.

$f_v = 2.1 \times 10^{-8}, R = 1.8 \times 10^6$ $(\eta_{high} = 1.06 \times 10^{-3})$			$f_v = 7.0 \times 10^{-7}, R = 9.3 \times 10^5$ $(\eta_{high} = 5.33 \times 10^{-4})$			$f_v = 5.7 \times 10^{-7}, R = 1.9 \times 10^5$ $(\eta_{high} = 1.02 \times 10^{-4})$		
element	high	average	element	high	average	element	high	average
⁵⁶ Ni	1.25×10^{-4}	4.55×10^{-6}	¹⁴² Nd	1.99×10^{-5}	1.22×10^{-6}	¹⁴⁵ Nd	3.69×10^{-7}	3.61×10^{-8}
⁵⁷ Co	1.59×10^{-5}	5.79×10^{-7}	⁵⁶ Ni	1.37×10^{-5}	8.35×10^{-7}	⁴⁰ Ca	2.71×10^{-7}	2.65×10^{-8}
⁸⁶ Sr	1.06×10^{-5}	3.86×10^{-7}	¹⁴⁶ Sm	1.03×10^{-5}	6.30×10^{-7}	⁵² Mn	2.42×10^{-7}	2.36×10^{-8}
⁸⁷ Sr	9.77×10^{-6}	3.56×10^{-7}	¹⁴⁵ Pm	8.91×10^{-6}	5.44×10^{-7}	¹⁵⁵ Eu	2.37×10^{-7}	2.32×10^{-8}
⁷⁴ Se	9.75×10^{-6}	3.55×10^{-7}	¹⁴⁸ Sm	8.25×10^{-6}	5.05×10^{-7}	¹⁴⁰ Ce	1.93×10^{-7}	1.89×10^{-8}
⁷⁵ Se	2.93×10^{-6}	1.07×10^{-7}	¹⁴⁷ Pm	6.62×10^{-6}	4.05×10^{-7}	⁵¹ Cr	1.55×10^{-7}	1.51×10^{-8}
⁷⁴ Sr	9.17×10^{-6}	3.34×10^{-7}	¹⁴⁴ Sm	5.24×10^{-6}	3.20×10^{-7}	¹⁴² Ce	1.11×10^{-7}	1.09×10^{-8}
⁸² Kr	8.91×10^{-6}	3.25×10^{-7}	¹⁴³ Pm	4.15×10^{-6}	2.54×10^{-7}	⁵⁶ Ni	1.10×10^{-7}	1.08×10^{-8}
⁸¹ Kr	7.80×10^{-6}	2.84×10^{-7}	¹⁴⁷ Sm	3.99×10^{-6}	2.44×10^{-7}	¹⁴⁶ Nd	1.05×10^{-7}	1.03×10^{-8}
⁷² Ge	7.67×10^{-6}	2.80×10^{-7}	¹⁴⁴ Pm	3.66×10^{-6}	2.24×10^{-7}	¹⁵⁶ Eu	9.44×10^{-8}	9.22×10^{-9}
⁷⁸ Kr	7.60×10^{-6}	2.77×10^{-7}	¹⁴⁶ Pm	3.46×10^{-6}	2.12×10^{-7}	¹⁴⁸ Nd	9.36×10^{-8}	9.15×10^{-9}
⁸⁰ Kr	7.06×10^{-6}	2.57×10^{-7}	¹⁴³ Nd	2.84×10^{-6}	1.74×10^{-7}	⁵² Fe	8.97×10^{-8}	8.77×10^{-9}
⁸³ Kr	6.25×10^{-6}	2.28×10^{-7}	¹⁴⁵ Sm	2.67×10^{-6}	1.63×10^{-7}	¹⁶¹ Tb	8.96×10^{-8}	8.52×10^{-9}
⁷³ Ge	6.14×10^{-6}	2.24×10^{-7}	¹⁴⁴ Nd	2.25×10^{-6}	1.37×10^{-7}	¹³⁹ La	8.80×10^{-8}	8.60×10^{-9}
⁷⁶ Se	5.93×10^{-6}	2.16×10^{-7}	¹⁴⁹ Sm	1.76×10^{-6}	1.07×10^{-7}	¹⁴ N	8.74×10^{-8}	8.54×10^{-9}
⁷⁹ Br	5.90×10^{-6}	2.15×10^{-7}	¹⁴⁸ Pm	1.16×10^{-6}	7.09×10^{-7}	⁴⁸ Cr	8.56×10^{-8}	8.39×10^{-9}
⁷⁷ Se	5.35×10^{-6}	1.95×10^{-7}	¹⁵⁰ Sm	9.88×10^{-7}	6.04×10^{-7}	¹³⁸ Ba	7.96×10^{-8}	7.77×10^{-9}
⁸⁹ Y	4.76×10^{-6}	1.73×10^{-7}	⁵⁷ Ni	7.52×10^{-7}	4.60×10^{-7}	¹² C	7.67×10^{-8}	7.50×10^{-9}
⁹⁰ Zr	4.41×10^{-6}	1.61×10^{-7}	¹⁰⁸ Cd	5.92×10^{-7}	3.62×10^{-7}	¹⁶² Dy	6.84×10^{-8}	6.68×10^{-9}
⁸⁵ Rb	4.32×10^{-6}	1.58×10^{-7}	¹⁵¹ Eu	5.30×10^{-7}	3.24×10^{-7}	¹³ C	6.43×10^{-8}	6.28×10^{-9}
⁸³ Rb	4.08×10^{-6}	1.49×10^{-7}	¹⁵³ Eu	5.23×10^{-7}	3.20×10^{-8}	¹⁶ O	6.30×10^{-8}	6.16×10^{-9}
⁸⁸ Y	3.85×10^{-6}	1.40×10^{-7}	¹¹⁰ Cd	4.70×10^{-7}	2.88×10^{-8}	¹⁵⁸ Gd	5.85×10^{-8}	5.71×10^{-9}
⁸⁸ Zr	3.55×10^{-6}	1.29×10^{-7}	¹⁴⁹ Eu	3.79×10^{-7}	2.32×10^{-8}	¹³⁷ Cs	5.56×10^{-8}	5.43×10^{-9}
⁷³ As	3.52×10^{-6}	1.28×10^{-7}	¹⁵² Eu	3.45×10^{-7}	2.11×10^{-8}	¹⁴⁷ Nd	3.96×10^{-8}	3.87×10^{-10}
⁷¹ Ga	3.40×10^{-6}	1.23×10^{-7}	¹⁴⁰ Ce	3.48×10^{-7}	2.12×10^{-8}	¹⁶⁵ Ho	3.77×10^{-8}	3.68×10^{-9}
⁷⁵ Se	2.93×10^{-6}	1.07×10^{-7}	¹⁵⁰ Eu	2.90×10^{-7}	1.77×10^{-8}	¹⁴³ Pr	3.11×10^{-8}	3.04×10^{-9}
⁹¹ Nb	2.90×10^{-6}	1.06×10^{-7}	²⁰⁶ Cd	2.89×10^{-7}	1.77×10^{-8}	¹⁴¹ Ce	3.00×10^{-8}	2.93×10^{-10}

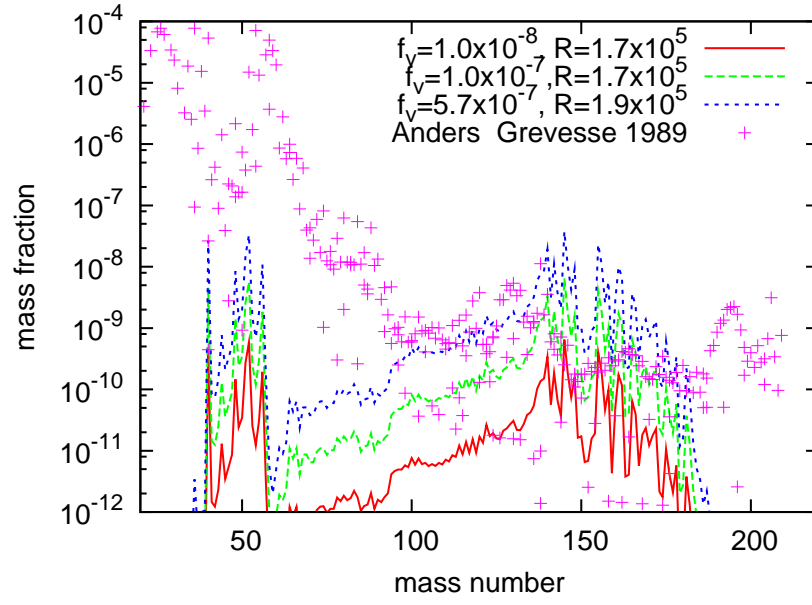


Fig. 9: Same as Fig. 8, but η_{high} is fixed as 10^{-4} .